Modeling turbulent flow from dam break using slow manifolds

D. J. Georgiev A. J. Roberts D. V. Strunin

June 4, 2009

Abstract

We present a novel approach based on centre manifold technique to describe the dynamics of the mean turbulent velocity of dam-break flow. We avoid empirical assumptions about the cross-stream profile of the velocity; instead solution is obtained using free surface and bed boundary conditions that accommodate constant turbulent shear as a nearly neutral mode. We describe the turbulent dynamics across the flow, and identify important factors affecting the turbulent dissipation in the lateral direction. The results are verified against available experimental data.

Contents

1 Introduction

Many environmental flows such as rivers, tidal waves and dam-breaks have low aspect ratio of the depth to lateral extent and fluid pressure is close to hydrostatic balance. Such flows are driven by gravity, which generates developed turbulence and reshapes the free surface. The dam-break flow is an example of such type of flow, where fluid is released from rest following

sudden removal of the lock. The dam-break flow has been studied for more than a hundred years, both theoretically [13] and experimentally [3]. Due to complexity of the modelling the theoretical models either adopt laminar or inviscid formulation, or use various empirical assumptions about the parameters of turbulence. There is a trend to replace these assumptions with DNS, LES [8] or dynamical system [12] approaches, as they allow a much deeper insight into the dynamics.

In this article we apply modern dynamical systems theory that empowers us to systematically control error, assess domains of validity, comprehensively account for further physical effects, and resolve internal structures within the dam-break flow. We aim the mathematics to represent the dominant physics: as indicated by Figures 14–15 by Janosi [3], turbulence does mix across the fluid layer. Thus, we expect to be able to model the dynamics in terms of depth-averaged quantities. But instead of crudely depth-averaging the equations, we use centre manifold theory to resolve turbulent dynamics across the fluid layer and hence provide a sound macroscale closure for the relatively slow, long term dynamics of interest to environmental modelers.

2 Problem formulation

Flow model We consider 2-D flow of incompressible fluid with constant density ρ, with lateral, $x_1 = x$, and normal, $x_3 = z$, directions on a slightly sloping ground, and thickness $\eta(x,t)$. The turbulence of the flow is assumed fully developed with mean velocity field $\boldsymbol{u} = (u, w) = (u_1, u_3)$. The related mean strain-rate tensor is

$$S_{ij} = \tfrac{1}{2}\left(\frac{\partial u_i}{\partial x_j} + \frac{\partial u_j}{\partial x_i}\right), \tag{1}$$

and its second invariant is

$$S = \left(\sum_{i,j} S_{ij}^2\right)^{1/2}. \tag{2}$$

Mass conservation is described by

$$\boldsymbol{\nabla}\cdot\boldsymbol{u} = \frac{\partial u}{\partial x} + \frac{\partial w}{\partial z} = 0\,, \tag{3}$$

and the transfer of momentum by

$$\frac{\partial \boldsymbol{u}}{\partial t} + \boldsymbol{u}\cdot\boldsymbol{\nabla}\boldsymbol{u} = -\boldsymbol{\nabla}p + \boldsymbol{\nabla}\cdot\boldsymbol{\tau} + \boldsymbol{g}\,, \tag{4}$$

where p is the mean pressure field and $\boldsymbol{\tau}$ is mean deviatoric stress tensor. The forcing of the flow $\boldsymbol{g} = (g_1, g_3)$ is from gravity.

Turbulence model The effects of turbulence are modeled with the eddy viscosity ν, which is related to the mean shear stress via the Boussinesq equation

$$\tau_{ij} = 2\ \nu\ S_{ij}\,. \tag{5}$$

We aim to model flows with very large Reynolds number using Smagorinski model of turbulence [8]. It sets the turbulent eddy viscosity ν to be proportional to S

$$\nu = l^2\ S\,, \tag{6}$$

where l is the length scale of mixing of turbulent eddies,

$$l = \eta\sqrt{c_t}\,, \tag{7}$$

and c_t is an empirical constant related to the strenght of the mixing. Relation (6) is vaid at certain distance from the boundaries. The resulting relation for the mean stress (5) is

$$\tau_{ij} = 2c_t\eta^2 S S_{ij} = c_t\eta^2 S\left(\frac{\partial u_i}{\partial x_j} + \frac{\partial u_j}{\partial x_i}\right)\,, \tag{8}$$

and together with (3) and (4) it governs the dynamical evolution of the flow. The quantities we want to determine are the flow thickness η and the mean velocity field $\boldsymbol{u}$.

Boundary conditions We set boundary conditions on the mean bed ($z = 0$) and on the free surface ($z = \eta$). The mean bed stops vertical movements so that

$$w = 0 \quad \text{and} \quad S = \frac{1}{\sqrt{2}}\frac{\partial u}{\partial z} \quad \text{on } z = 0\,, \tag{9}$$

but allows slip to account for a relatively thin turbulent boundary layer,

$$u = c_u\,\eta\,\frac{\partial u}{\partial z} \quad \text{on } z = 0\,. \tag{10}$$

The physical meaning of (10) is that the mean bed $z = 0$ is located at the lower edge of the turbulent boundary layer where there is no mean flow in the vertical direction, but the mean flow in lateral direction is proportional to the friction velocity u_*,

$$u \propto u_* \quad \text{on } z = 0\,, \tag{11}$$

where $u_* \equiv \sqrt{\mu\ \frac{\partial u}{\partial z}\big|_{z=0}}$, and μ is the molecular viscosity. At $z = 0$ the viscous and turbulent effects are assumed approximately equal, therefore $\mu \approx \nu|_{z=0}$

and the friction velocity is defined as $u_* = \sqrt{\nu|_{z=0}\,\frac{\partial u}{\partial z}\big|_{z=0}}$. From (11), taking into account (9), (6) and (7), we obtain (10). The value of the constant c_u depends on the proportionality (11) and has to be defined empirically similarly to c_t; in such a way the parameter $c_u\,\eta$ in (10) evaluates the "slip length" on the bed.

At $z = \eta$ we have the mean free surface, and the kinematic condition there is

$$\frac{\partial \eta}{\partial t} + u\frac{\partial \eta}{\partial x} = w \quad \text{on } z = \eta\,. \tag{12}$$

Also, assuming that the atmospheric pressure is zero in our system of units, the turbulent mean stress normal to the free surface is also zero,

$$-\,p + \frac{1}{1+\eta_x^2}\left(\tau_{33} - 2\eta_x\tau_{13} + \eta_x^2\tau_{11}\right) = 0 \quad \text{on } z = \eta\,. \tag{13}$$

Lastly, there must be no turbulent mean tangential stress at the free surface:

$$(1-\eta_x^2)\tau_{13} + \eta_x(\tau_{33} - \tau_{11}) = 0 \quad \text{on } z = \eta\,. \tag{14}$$

3 Centre manifold technique

We proceed to solve the governing equations of the flow (3), (4) and (8) by applying a new approach based on centre manifold theory. As we mentioned, our primary interest is the time evolution of the height of the flow $\eta(x,t)$ and depth averaged lateral velocity $\bar{u}(x,t) = 1/\eta\int_0^\eta u dz$. However, we do not assume that $u(z)$ is known empirically, instead we use the centre manifold theory to resolve turbulent dynamics across the fluid layer by separating the influence of the terms involved in (3)–(4), (8) on the basis of their time scales. In such a way the relatively slow, long term dynamics of turbulent mixing and the preservation of mass are recognized as dominant, and the lateral derivatives $\partial_x^n \equiv \left[\frac{\partial^n \bar{u}}{\partial x^n}\,,\frac{\partial^n \eta}{\partial x^n}\right]$, the gravitational forcing $\boldsymbol{g}$ and the curvature of the free surface, are recognized as imposed perturbations.

To implement this approach we need to provide special mechanism in (3)–(4), (8) and/or in the boundary conditions, such that these equations are solved by a family of shear flows and with constant thickness. On this basis two neutral modes of the dynamics of the flow can be defined, and the space of equilibria of (3)–(4), (8) can be parameterized using $\bar{u}(x)$ and $\eta(x)$. To allow this we add an artificial tangential stress on the free surface, proportional to the local velocity $u^2(\eta)$. The boundary condition (14) is replaced by

$$(1-\eta_x^2)\tau_{13} + \eta_x(\tau_{33} - \tau_{11}) = \frac{(1-\gamma)c_t}{\sqrt{2}(1+c_u)^2}u^2 \quad \text{on } z = \eta\,, \tag{15}$$

where γ is an artificial parameter ranging from zero to one. When $\gamma = 1$ the physical boundary condition (14) is recovered. However, when $\gamma = 0$ and $g_1 = \partial_x = 0$, then from (5) $\tau_{13} = \nu\,\partial u/\partial z$ and, hence, the artificial free surface condition (15) reduces to $u = (1 + c_u)\,\eta\,\partial u/\partial z$ on $z = \eta$. As a result, when $\gamma = 0$ then (10) and (15) define artificial shear flow $u \propto c_u + \zeta$, where ζ is the scaled normal coordinate, namely

$$u(x, z, t) = \bar{u}(x, t)\,\frac{c_u + \zeta}{c_u + \frac{1}{2}}\,, \quad \zeta \equiv z/\eta\,. \tag{16}$$

In such a way the first neutral mode of the dynamics is defined. Conservation of fluid provides the second neutral mode: when $\gamma = g_1 = \partial_x = 0$ then $\eta = \text{const}$. Thus when $\gamma = g_1 = \partial_x = 0$, there is a two-parameter family of equilibria corresponding to some uniform shear flow, $u \propto c_u + \zeta$, of any constant thickness η. For large enough lateral length scales, these equilibria occur independently at each location x [9, 10] and hence the space of equilibria are in effect parametrized by $\bar{u}(x)$ and $\eta(x)$. Provided we can treat lateral derivatives ∂_x as a modifying influence, that is provided solutions vary slowly enough in x, centre manifold theorems [1, 5] assure us that the evolution of the system (3)–(4), (8) develops on a slow manifold with the following properties:

- It is a perturbation of the subspace of equilibria;
- It *exists for a finite range* of parameters ∂_x, γ and g_1;
- It is parametrized by the average $\bar{u}(x, t)$ and $\eta(x, t)$, therefore the evolution on it is low dimensional;
- It *attracts solutions from all nearby initial conditions* exponentially quickly;
- It may be *approximated* by power series in ∂_x, γ and g_1 to the same order of error as the governing PDEs.

The slow manifold is constructed using asymptotic series and computer algebra. The details of the algorithm can be found in Roberts [11]. The cross fluid structure of the velocity, pressure and strain rate forms the slow manifold, here with no lateral variations, $\partial_x = 0$, as we compare with uniform flow. The result for lateral velocity shear profile is

$$u \;=\; \bar{u}\,\frac{c_u + \zeta}{c_u + \frac{1}{2}} + \gamma\bar{u}\,\frac{(1 + c_u)[(1 + 4c_u)(c_u + \zeta) - 2(1 + 2c_u)(3c_u\zeta^2 + \zeta^3)]}{4(1 + 2c_u)^2(1 + 3c_u + 3c_u^2)}$$

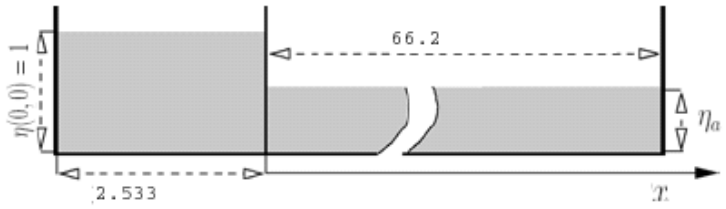

Figure 1: Schematic arrangement and geometric dimensions of the dam-break experiments of Janosi et al. [3].

$$+\frac{g_1\eta}{\bar{u}}\frac{[(5+6c_u)(c_u+\zeta)-6(2+7c_u+6c_u^2)\zeta^2+6(1+2c_u)^2\zeta^3]}{48\sqrt{2}\,c_t(1+3c_u+3c_u^2)}$$
$$+\mathcal{O}\big(\gamma^2+g_1^2+\partial_x\big)\,, \tag{17}$$

and the magnitude of the rate of strain tensor is

$$\begin{aligned} S &= \frac{\bar{u}}{\eta}\frac{\sqrt{2}}{1+2c_u}+\frac{\gamma\bar{u}}{\eta}\frac{\sqrt{2}(1+c_u)[(1+4c_u)-6(1+2c_u)(2c_u\zeta+\zeta^2)]}{8(1+2c_u)^2(1+3c_u+3c_u^2)} \\ &\quad +\frac{g_x}{\bar{u}}\frac{[(5+6c_u)-12(2+7c_u)\zeta+18(1+2c_u)^2\zeta^2]}{96c_t(1+3c_u+3c_u^2)} \\ &\quad +\mathcal{O}\big(\gamma^2+g_1^2+\partial_x\big)\,, \end{aligned} \tag{18}$$

for flow with hydrostatic pressure $p = g_3\,\eta(1-\zeta)$. The corresponding evolution of the mean lateral velocity is

$$\begin{aligned} \frac{d\bar{u}}{dt} &= -\frac{\sqrt{2}\,3c_t(1+c_u)}{(1+2c_u)(1+3c_u+3c_u^2)}\frac{\gamma\bar{u}^2}{\eta}+\frac{\frac{3}{4}+3c_u+3c_u^2}{1+3c_u+3c_u^2}g_1 \\ &\quad +\mathcal{O}\big(\gamma^2+g_1^2+\partial_x\big)\,. \end{aligned} \tag{19}$$

To obtain a physical model from (17)–(19) we set the artificial parameter $\gamma = 1$. Then (17)–(19) describe the equilibrium of an uniform open channel flow, e.g. the second term in (19) accelerates the flow by the lateral gravitational forcing, until is balanced by dissipation, the first term.

4 Calibration

We construct the slow manifold for small lateral derivatives, small lateral forcing and small perturbation of the free surface condition. Later we analyze the time evolution of $\eta(x,t)$ and $\bar{u}(x,t)$ to verify that these criteria are satisfied for the specific flow of interest. However, (17)–(19) with $\gamma = 1$

describe a family of equilibrium flows, therefore firstly the Smagorinsky 'mixing' coefficient c_t and bed 'slip' coefficient c_u have to be set to appropriate values which correspond to a specific uniform flow with fully developed turbulence. Then (17)–(19) with $\gamma = 1$ will describe the lateral velocity shear profile and equilibrium of such flow since they were derived assuming no lateral variations $\partial_x = 0$.

The stationary channel flow is closest to these assumptions, it is well studied and there are experimental data showing the structure of the turbulence in the interior of the flow. Summarizing many experiments, Nezu [7] gave empirical formulae for the structure of the turbulent energy $k(z) = 4.78\, u_*^2 \exp(-2\zeta)$ and dissipation $\epsilon(z) = 9.8\, u_*^3 \exp(-3\zeta)/(\eta\sqrt{\zeta})$; from these one can find the profile of the eddy viscosity $\nu(z) = C_\mu k^2/\epsilon$, thus the depth averaged eddy viscosity is $\bar{\nu} = 0.0796\, \eta u_*$. From (17)–(19) these depth averaged flow parameters can be estimated, for example the mean velocity is

$$\bar{u} = \frac{1}{2}\left[\frac{(1+2c_u)^3}{c_t\sqrt{2}(1+c_u)}\right]^{\frac{1}{2}} \sqrt{g_1\eta}\,. \tag{20}$$

By choosing $c_t = 1/50$ and $c_u = 11/6$ this equilibrium velocity and the average eddy viscosity correspond to the empirical results, taking into account that $u_* = \sqrt{g_1\eta}$ for stationary channel flow driven only by the force of gravity.

Our next step is to estimate the spatio-temporal dynamics of non-stationary channel flow. In our model they are described by the time evolution of the flow height $\eta(x,t)$ and the depth-averaged lateral velocity $\bar{u}(x,t)$. They come as a result of taking into account the relatively slow variations in lateral direction x, and small but non-zero ∂_x, therefore these functions are smooth and slow in x. Strictly speaking, these dynamics are not lying on the centre manifold, but on a nearby slow manifold, see Georgiev et al. [2] for more details on such departures. The resulting $\eta(x,t)$ and $\bar{u}(x,t)$ are described by the conservation equation

$$\frac{\partial\eta}{\partial t} + \frac{\partial}{\partial x}(\eta\bar{u}) = 0\,, \tag{21}$$

and the momentum equation

$$\begin{aligned}\frac{\partial\bar{u}}{\partial t} = \quad & -1.045\,\bar{u}\tfrac{\partial\bar{u}}{\partial x} - 0.00311\,\gamma|\bar{u}|\bar{u}/\eta + 0.985\left(g_1 - g_3\tfrac{\partial\eta}{\partial x}\right) \\ & + 0.058\,\eta\tfrac{\partial|\bar{u}|}{\partial x}\tfrac{\partial\bar{u}}{\partial x} + 0.259\,\eta|\bar{u}|\tfrac{\partial^2\bar{u}}{\partial x^2} + 0.522\,|\bar{u}|\tfrac{\partial\eta}{\partial x}\tfrac{\partial\bar{u}}{\partial x} \\ & - 0.015\,\bar{u}^2\tfrac{\partial\eta}{\partial x}/\eta - 0.007\,|\bar{u}|\bar{u}\left(\tfrac{\partial\eta}{\partial x}\right)^2/\eta - 0.007\,|\bar{u}|\bar{u}\tfrac{\partial^2\eta}{\partial x^2} \\ & + \mathcal{O}\left(\gamma^{3/2} + g_1^{3/2} + g_3^3 + \partial_x^3\right). \end{aligned} \tag{22}$$

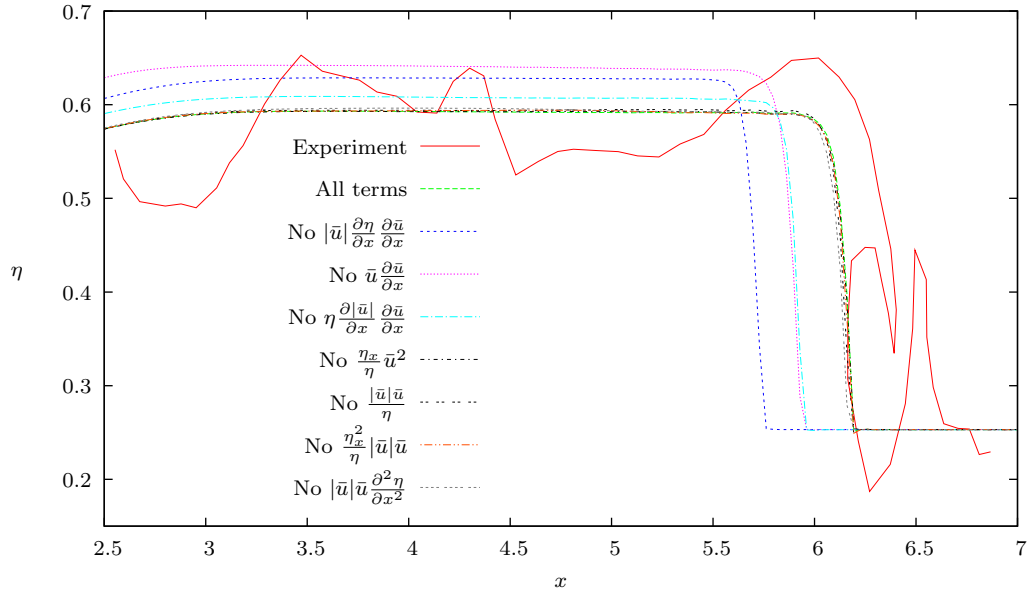

Figure 2: Comparison of experimental and computed η for $\eta_a = 0.253$ and $t = 4.794$.

Equation (22) contains inertial term $\bar{u}_t$, self-advection term $\bar{u}\frac{\partial\bar{u}}{\partial x}$, bed drag $|\bar{u}|\bar{u}/\eta$, gravitational forcing $g_1 - g_3\frac{\partial\eta}{\partial x}$, and other terms related to turbulent mixing in lateral direction. We emphasize that the coefficients at these terms are derived using the centre manifold technique instead of using empirical relations, such as Chezy law for bed drag. Remarkably, in our model (22) the coefficient of gravitational forcing lessen the effect of gravity by 1-2%, and there are observations confirming that (see Roberts et al.[12]).

Applying (21)–(22) to dam-break flow, it is interesting to estimate the relative role of these terms in the evolution of $\eta(x,t)$. In doing so we use the experimental results of Janosi et al. [3] on dam-break flow. The experimental setting is shown in Figure 1. The initial filling height is assumed $\eta(0,0) = 1$ in our system of units, $g_3 = 1$, the lock begins to open at $t = 0$ and is fully opened at $t = 0.808$. We focus on two runs with $Re \approx 30,000$–$40,000$, ambient height of the flow being $\eta_a = 0.12$ and $\eta_a = 0.253$. During these laboratory experiments various phenomena related to intensive turbulent mixing were observed. They are: developed propagating bore, air bubbles, surface wave breaking in forward and inverse directions, and an unstable mushroom-like surface wave, which was also reported by Stansby et al. [13].

During the experiments snapshots were taken of the water height $\eta(x,t)$ for consecutive moments of time [3]. We choose to compare $\eta(x,t)$ from

our modeling with the experimental $\eta(x,t)$, rather than compare $\bar{u}(x,t)$, since the observations of the height of the flow are more precise than the measurements of the mean velocity. Equations (21) and (22) are solved numerically using EPDCOL solver of PDEs created by Keast and Muir [4], which is a successor of PDECOL solver of Madsen and Sincovec [6]; it employs a collocation based method-of-lines approach. In Figure 2 a comparison of the height of the flow is shown for the most distant moment of time. To estimate the relative role of the terms in (22), the profile of η is calculated with some of the terms omitted (except for the gravitational forcing and $\eta|\bar{u}|\frac{\partial^2\bar{u}}{\partial x^2}$), and compared with the solution produced using all the terms of (22). We found that apart from the self-advection term $\bar{u}\frac{\partial\bar{u}}{\partial x}$, only the two terms $|\bar{u}|\frac{\partial\eta}{\partial x}\frac{\partial\bar{u}}{\partial x}$ and $\eta\frac{\partial|\bar{u}|}{\partial x}\frac{\partial\bar{u}}{\partial x}$ have a significant effect on the lateral speed of the water front, these terms are related to turbulent mixing in lateral direction. Thus, the terms representing turbulent mixing in the third line of (22) are not significant, and (22) can be simplified to

$$\begin{aligned}\frac{\partial\bar{u}}{\partial t} \approx \quad & -1.045\,\bar{u}\frac{\partial\bar{u}}{\partial x} - 0.00311\,|\bar{u}|\bar{u}/\eta + 0.985\left(g_1 - g_3\frac{\partial\eta}{\partial x}\right) \\ & + 0.058\,\eta\frac{\partial|\bar{u}|}{\partial x}\frac{\partial\bar{u}}{\partial x} + 0.259\,\eta|\bar{u}|\frac{\partial^2\bar{u}}{\partial x^2} + 0.522\,|\bar{u}|\frac{\partial\eta}{\partial x}\frac{\partial\bar{u}}{\partial x}\,. \end{aligned} \tag{23}$$

Equation (23) is obtained using $\gamma = 1$ to restore the physical boundary condition (14) on the free surface. This relation can be simplified further by approximating the coefficients to two decimals and combining the last three terms into one:

$$\begin{aligned}\frac{\partial\bar{u}}{\partial t} + 1.05\,\bar{u}\frac{\partial\bar{u}}{\partial x} \approx \quad & -0.0031|\bar{u}|\bar{u}/\eta + 0.98\left(g_1 - g_3\frac{\partial\eta}{\partial x}\right) \\ & + 0.26\frac{|\bar{u}|^{0.78}}{\eta}\frac{\partial}{\partial x}\left(\eta^2|\bar{u}|^{0.22}\frac{\partial\bar{u}}{\partial x}\right)\,. \end{aligned} \tag{24}$$

This equation accumulates the influence of the three major factors: bed drag, gravitational forcing and turbulent dissipation in lateral direction. We reiterate that the models (23) and (24) are not derived by depth-averaging, but by using centre manifold theory, which systematically accounts for interactions of vertical profiles of the velocity/stress and bed drag with lateral space variations. This approach provides a solid ground for regularizing the dissipation in the second lines of (23) and (24).

5 Dam-break modeling

In Figures 3 and 4 the computed profiles of the dam-break flow for ambient heights $\eta_a = 0.12$ and $\eta_a = 0.253$ are compared with snapshots from the experiments. When $\eta_a = 0.12$ the static layer at the bottom is thinner and its

interaction with the propagating bore causes wave breaking and entrainment of air bubbles. In our modeling we assume that the lock was fully opened at $t = 0$, and, as a consequence, the computed front of the flow is ahead of the experimental one at early moments of time; later the speed of the two fronts become close. Note that the experimental snapshots show instantaneous height of the flow, while we computed the ensemble average height. Therefore we do not expect to reproduce fine details of the transient turbulent strictures, such as mushroom-like surface wave, wave breaking and air bubbles. They are highly curved and therefore are far from being small perturbations of the free surface. Nevertheless, not far behind the propagating bore the profile of the surface is smoother and its ensemble-average is close to the computed profile.

When the static layer at the bottom is thick ($\eta_a = 0.253$), its interaction with the propagating bore is delayed and so is the wave breaking in forward direction. There are no captured air bubbles, and the mushroom-like surface wave is larger and smoother. As a result, the correspondence with the computed profile is better and the computed front is closer to the propagating bore. In backward direction the computed profile is close to the ensemble-averaged experimental profile.

References

[1] J. Carr. *Applications of centre manifold theory*, volume 35 of *Applied Mathematical Sciences*. Springer-Verlag, 1981.

[2] D.J. Georgiev, A.J. Roberts, and D.V. Strunin. Nonlinear dynamics on centre manifolds describing turbulent floods: k-ω model. *Discrete and Continuous Dynamical Systems Supplements*, (Special):419–428, 2007. `http://aimsciences.org/journals/pdfs.jsp?paperID=2848&mode=full`.

[3] I.M. Janosi, D. Jan, K.G. Szabo, and T. Tel. Turbulent drag reduction in dam-break flows. *Experiments in Fluids*, 37:219–229, 2004.

[4] P. Keast and P.H. Muir. EPDCOL: A more efficient PDECOL code. *ACM Transactions on Mathematical Software*, 17(2):153–166, 1991.

[5] Y.A. Kuznetsov. *Elements of applied bifurcation theory*, volume 112 of *Applied Mathematical Sciences*. Springer-Verlag, 1995.

[6] N.K. Madsen and R.F. Sincovec. PDECOL: General collocation software for partial differential equations. *ACM Transactions on Mathematical Software*, 5(3):326–351, 1979.

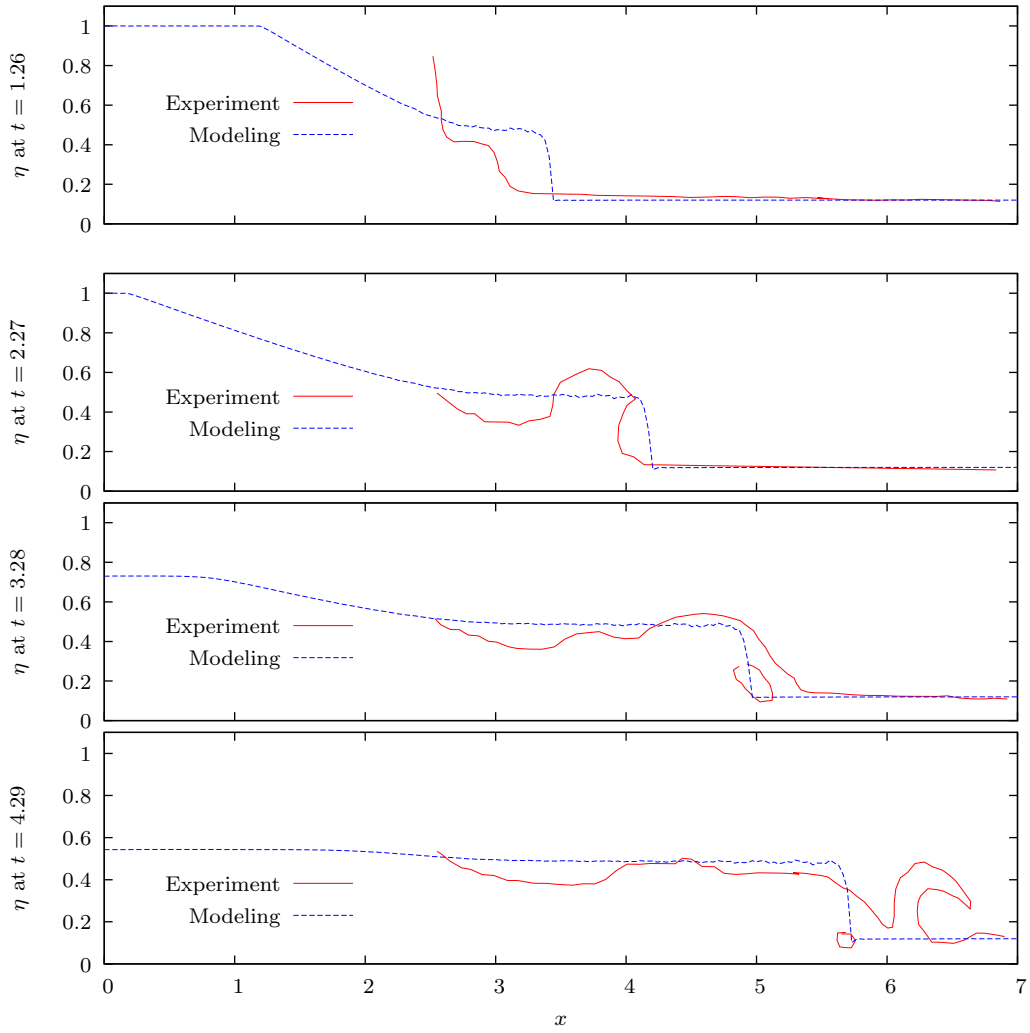

Figure 3: Comparison of experimental and computed η for $\eta_a = 0.12$

[7] I. Nezu. Open-channel flow turbulence and its research prospects in the 21st century. *Journal of Hydraulic Engineering*, 131(4):229–246, April 2005.

[8] T.M. Özgökmen, T. Iliescu, P.F. Fischer, A. Srinivasan, and J. Duan. Large eddy simulation of stratified mixing and two-dimensional dam-break problem in a rectagular enclosed domain. *Ocean Modelling*, 16:106–140, 2007.

[9] A.J. Roberts. The application of centre manifold theory to the evolution of systems which vary slowly in space. *Journal of Australian Mathematical Society B*, 29:480–500, April 1988.

[10] A.J. Roberts. Low-dimensional modelling of dynamics via computer algebra. *Computer Physics Communications*, 100:215–230, 1997.

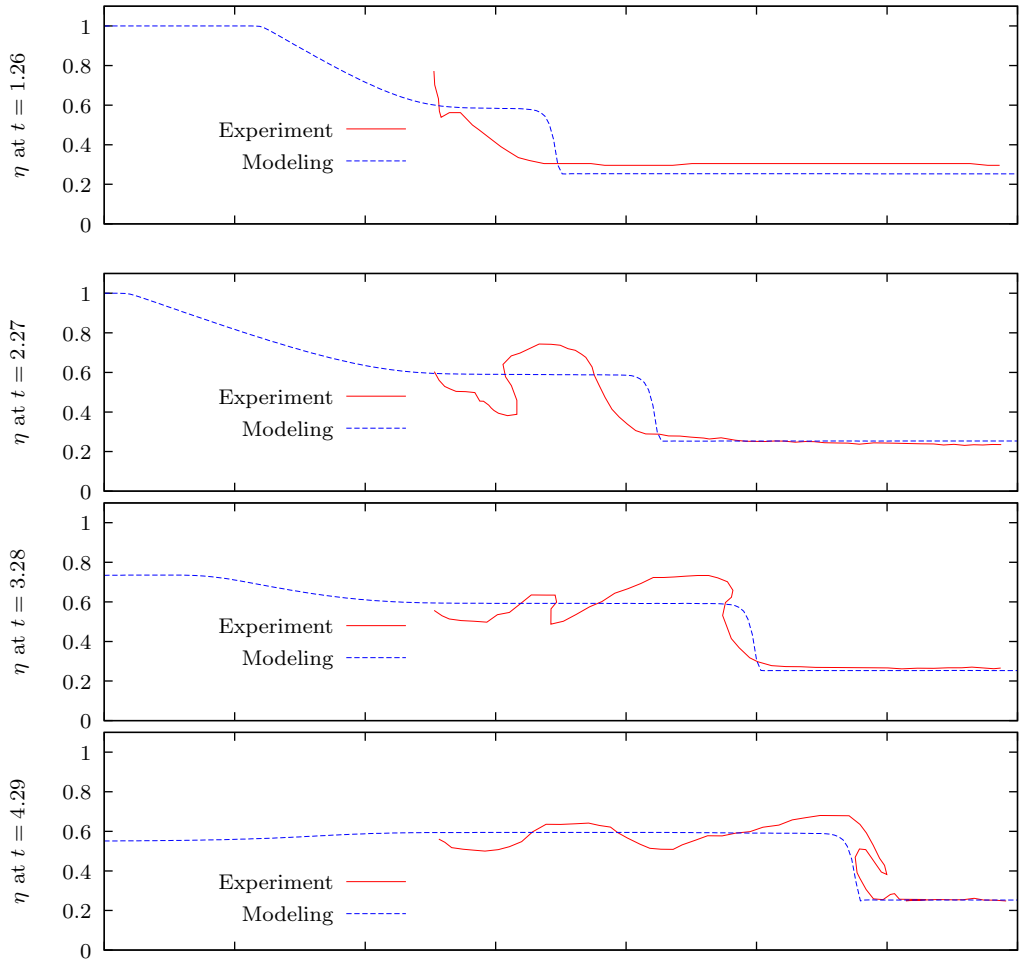

Figure 4: Comparison of experimental and computed η for $\eta_a = 0.253$

[11] A.J. Roberts. Computer algebra describes flow of turbulent floods via the Smagorinsky large eddy closure. Technical report, University of Southern Queensland, 2008. `http://eprints.usq.edu.au/4008/`.

[12] A.J. Roberts, D.J. Georgiev, and D.V. Strunin. Model turbulent floods with the Smagorinski large eddy closure. `http://arxiv.org/abs/0805.3192/`.

[13] P.K. Stansby, A. Chegini, and T.C.D. Barnes. The initial stages of dam-break flow. *Journal of Fluid Mechanics*, 374:407–424, 1998.